MEGA JOURNAL OF CASE REPORTS

OPEN ACCESS

Research Article

Compiled Date: September 18, 2025

High-Sensitivity Diamond-tipped Thermal Sensor for Non-Invasive Skin Cancer Detection: Development and Validation – Part A

Nathalie Nick, Joe Kirkup, and Kam Chana

University of Oxford, Department of Engineering Science, Parks Road, Oxford, OX13PJ, UK

***Corresponding author**: Nathalie Nick, University of Oxford, Department of Engineering Science, Oxford, OX13PJ, UK

Abstract

A novel diamond-tipped thermal sensor has been developed for non-invasive skin cancer detection. The device uses a single-crystal diamond substrate with a thermocouple measurement, modelling demonstrates a ~10 times sensitivity improvement (0.08°C/thermal product) over previous thin-film thermal product sensors. Part A of this 2-part paper details the sensor concept, modelling of the sensor for various materials, and design rationale. Part B paper presents experimental validation, statistical modelling, and preliminary biological tissue testing.

Keywords: Thermal product sensor; Diamond substrate; Skin cancer detection; Non-invasive diagnostics; Thermal properties; Biomedical sensing

Introduction

Skin cancer is among the most prevalent cancers worldwide, with melanoma cases in the UK alone rising by 140% since the early 1990s to over 16,000 annual diagnoses [1]. Current diagnostic pathways rely heavily on visual inspection followed by a biopsy, a process associated with high costs and significant over-referral, with approximately 12 benign lesions excised for every confirmed melanoma [2,3]. Thermal sensing provides a promising non-invasive diagnostic alternative, exploiting differences in thermal product (TP), $\sqrt{(\rho ck)}$, where ρ is density, c specific heat capacity, and k thermal conductivity. Thin-film thermal product sensors have demonstrated proof-of-concept success in distinguishing cancerous from healthy tissue [6], including 100% accuracy in a 12-patient clinical trial, but were limited by fragile sensor construction, lower sensitivity (0.001037°C/TP), and direct electrical contact risks [4-6]. The investigation reported in this paper gives the development of a diamond-tipped thermal sensor that fundamentally overcomes these limitations. Diamond has exceptional thermal properties ($\sqrt{(\rho ck)}$, ≈55,954 J/(m^2 K s$^{0.5}$)), mechanical robustness, electrical insulation, and biocompatibility enables a new sensor concept with enhanced sensitivity, inherent safety, and ultimate durability. This study is reported in a two-part

paper, Part A describes the materials modelling, conceptual design, and sensor architecture, establishing the rationale for a diamond-tipped approach. Part B presents complementary experimental validation, uncertainty analysis, demonstrating an order of magnitude sensitivity gain over previous sensors, predictive statistical modelling, and preliminary porcine testing.

Background

Thermal Product Measurement Principle

The working principle of a thermal product (√(ρck), also called thermal effusivity) measurement is based on the heat transfer relationship between a sensor and the material in contact with it. When a short heat pulse is generated within the sensor, it dissipates through both the sensor substrate and into the material in contact with the sensor. The temperature response measured at the sensor and target material interface can be directly correlated with the thermal properties of the contact material.

The fundamental relationship is governed by the one-dimensional transient heat conduction equation:

$$\frac{\partial^2 T(x,t)}{\partial x^2} = \frac{1}{\alpha(x)} \frac{\partial T(x,t)}{\partial t} \qquad \text{(Eq. 1)}$$

Where $\alpha(x) = \frac{k}{\rho c}$ is the thermal diffusivity. For a step change in temperature, the heat transfer rate is:

$$\dot{q}_{wall} = [T_{wall}(t) - T_0] \frac{\sqrt{\pi}}{2} \frac{\sqrt{\rho c k}}{\sqrt{t}} \qquad \text{(Eq. 2)}$$

This entails the heat transfer rate into the substrate $\dot{q}_{wall} \propto \sqrt{\rho c k}$, establishing the direct relationship between heat transfer rate and thermal product.

Previous Sensor: Thin Film-Based Approach

The thermal product sensing concept, originally developed at Oxford University (Patent number: 10585057. Filed: December 16, 2015. Granted: March 10, 2020) was initially demonstrated and validated on biological tissue [7] using a platinum thin film gauge-based sensor on an 8 mm diameter Macor[1] substrate **(Figure 1 left)**, where an electrical pulse generated the heat through the same thin film that measured the temperature response. The sensor was originally developed and applied in aerospace for oil contamination and debris detection. For further details of how this sensor operates see **[8].** In later trials **[6],** the same sensor was used on human skin lesions and distinguished between cancerous and healthy skin tissue based on thermal properties. Cancerous lesions, with increased porosity and altered architecture, exhibited lower density and reduced thermal product measurements (√ρck) compared to healthy tissue **(Figure 1 right).** This enabled 100% success in a 12-patient clinical study at Brighton General Hospital. The procedure for using this sensor was as follows: the sensor was initially calibrated using air and purified water, then thermal product measurements were taken of normal skin surrounding the mole and abnormal skin from the mole and, the difference has been evaluated. A negative thermal product difference was taken as non-cancerous tissue and a positive difference as cancerous tissue **(Figure 2).** This resulted in a 100% correlation with histopathological results that were subsequently obtained. The sensor sensitivity [°C/TP] of the thin film sensor used in these trials was measured at 0.001037°C/TP. The sensor required only two wires, which is an advantage, as the film that applies the heat does the measurement at the same time.

[1]MACOR is a Trade name for the machinable glass substrate

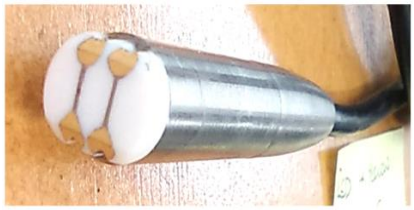

ø 8mm
6mm transducers

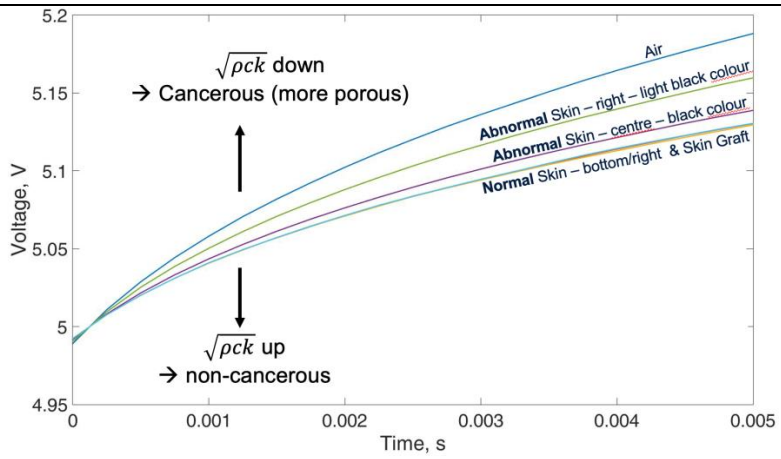

Figure 1: Thin film-based sensor with 8 mm diameter and 6 mm transducers (left) and the voltage curves of normal skin, abnormal skin, and air generated (right).

Patient	Skin issue from histology	Normal skin thermal product	Abnormal skin thermal product	Difference in Thermal product
1	Lentigo Maligna	560	361	199
2	Nodular BCC	859	826	33
3	Lentigo Maligna Melanoma	762	379	383
4	Scarring post SCC excision	289	443	-154
5	Scarring previous melanoma	677	450	227
6	Scarring previous melanoma	1000	1206	-206
7	Lentigo Maligna Melanoma	687	331	356
8	Lentigo Maligna	718	443	275
9	Scarring previous melanoma	787	693	94
10	scarring previous melanoma	248	286	-38
11	Bowenoid actinic keratosis	531	860	-329
12	Malignant Melanoma	680	650	30

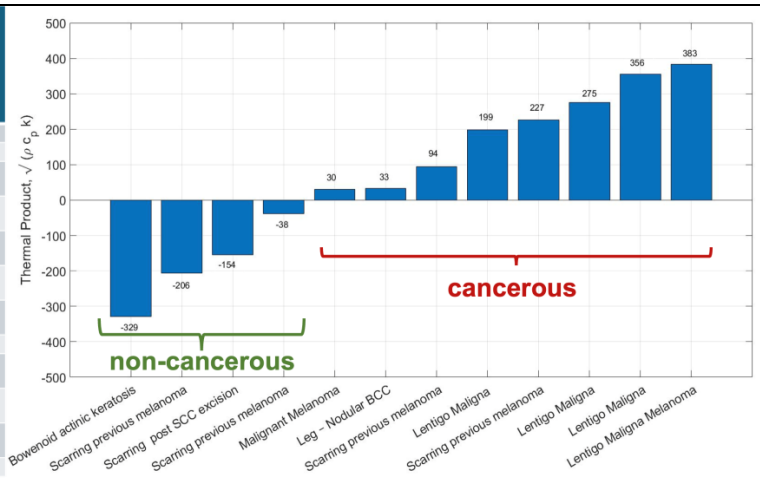

Figure 2: Result of 12-patient trial: tabulated thermal product (left) and histogram (right) highlighting that the thermal product differences of non-cancerous results were negative, while cancerous were positive.

Thin Film Approach: Advantages and Shortcomings

The original thin film sensor established thermal product sensing as a viable diagnostic technique. Despite clinical success, the thin film sensor presented limitations for routine use which included: direct electrical contact with tissue created safety concerns for on-patient applications, contamination risk required sterilisation between uses, fragile platinum films were susceptible to damage during general cleaning (alcohol wipe), and complex manufacturing processes. A critical limitation was indirect temperature measurement – the system measured voltage with a constant current circuit requiring conversion using a calibrated temperature coefficient of resistance (σ = 0.0053 V/°C).

Medical Film Integration: Findings and Limitations

To address electrical safety concerns, [4] investigated the use of a thin 47 μm medical plastic

film on the sensor surface for electrical isolation between the sensor and the patient tissue. For porcine skin, the film introduced only 1.7% measurement deviation. However, fat and muscle tissues exhibited substantial errors of 6.4% and 10.7% respectively, caused by uneven surfaces creating air gaps, electrical isolation effects reducing shorting, and film creasing creating inconsistent thicknesses.

Motivation for Improved Sensor Design

Limitations requiring improvement for clinical implementation were identified as: the need for external electrical isolation, poor resolution due to the size of the thin film gauges, and voltage-to-temperature conversion requirements. Additionally, the Macor substrate thermal product (≈ 1700 J/(m^2 K s$^{0.5}$)) versus skin tissue (≈ 700 to 1200 J/(m^2 K s$^{0.5}$)) meant significant thermal energy was conducted into the Macor substrate rather than into the tissue, demonstrated schematically in **Figure 3**.

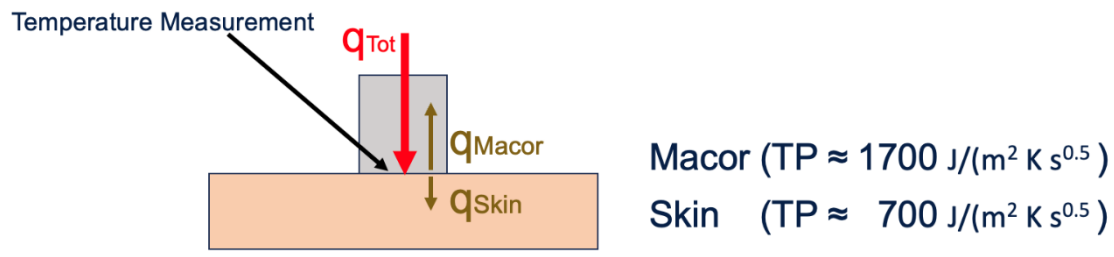

Figure 3: Location of both heat input and temperature measurement for thin film gauge sensor at the Macor-skin interface.

Theoretically, the power requirement at the skin–Macor interface follows an approximate 70:30 distribution when neglecting heat losses through the wires.

Novel Diamond-tipped Sensor Concept

Material Selection Criteria

Various materials were evaluated based on electrical insulation, durability, hardness, safety, and thermal performance. Because heat transfer rate is proportional to the thermal product ($\sqrt{\rho ck}$), candidates with high thermal product were prioritised. The investigation focused on dielectric materials offering electrical isolation alongside high thermal conductivity and mechanical hardness. These included single crystal diamond, sapphire, machinable glass, and aluminium oxide. Stainless steel 316 was considered as a non-dielectric reference. All material properties are summarised in **Table 1** with the values quotes being estimates only. Additional properties examined include temperature stability, environmental resistance, and machinability.

Table 1: Candidate sensor substrate materials.

Material	Thermal Product [J/(m^2 K s$^{0.5}$)]	Density [kg/m^3]	Specific Heat [J/kgK]	Thermal Conductivity [W/mK]	Vickers Hardness (kgf/mm^2)	Other Material Characteristics
Single Crystal Diamond	55,954	3,515	510-540	1,500-1,900	~10,000	Chemically Inert Biocompatible UV–IR Transparent
Macor (Machinable Glass Ceramic)	1,716	2,520	774-805	1.4-1.6	~250	Machinable Good Dielectric
Borosilicate Glass	1,427	2,230	830	1.0-1.2	~500-600	UV–IR Transparent, Good Dielectric Brittle
Sapphire (α-Al_2O_3)	10,927	3,980	750	40.0	~2,000	Chemically Inert UV–IR Transparent Good Dielectric
Aluminium Oxide (Alumina/Al_2O_3)	8,159	3,400-4,100	451-955	12.0-38.5	1,800-2,000	Excellent Dielectric Chemically Stable
Stainless Steel 316	8,050	8,000	500	16.2	~150–190	Non-Dielectric Reference Only

Heat Split Numerical Modelling

A simple one-dimensional (1D) thermal model was created using MATLAB 2022a simulating heat diffusion through the substrate materials detailed in **Table 1**. This model utilised MATLAB's "PDEPE function" which uses the "method of lines": spatial discretisation combined with temporal solving via a variable order implicit Runge-Kutta method. The primary objective of this analysis was to aid in classifying the materials, specifically to examine the "heat split ratio" between the polyimide body and substrate. This factor would have a significant effect on the input power required to achieve the maximum "on-skin temperature" of 42°C (see Section 3.3 for details).

The governing equation is like Eq.1 in all spatial domains, with a source term being included in the time interval $t_{delay} < t \leq t_{delay} + t_{pulse}$. The source term takes the form $\frac{q_0}{V_{wire}}$ where q_0 is the ohmic heating power and V_{wire} is the volume of the heater wire.

An abstracted diagram of the continuous spatial domain can be seen in **Figure 4**.

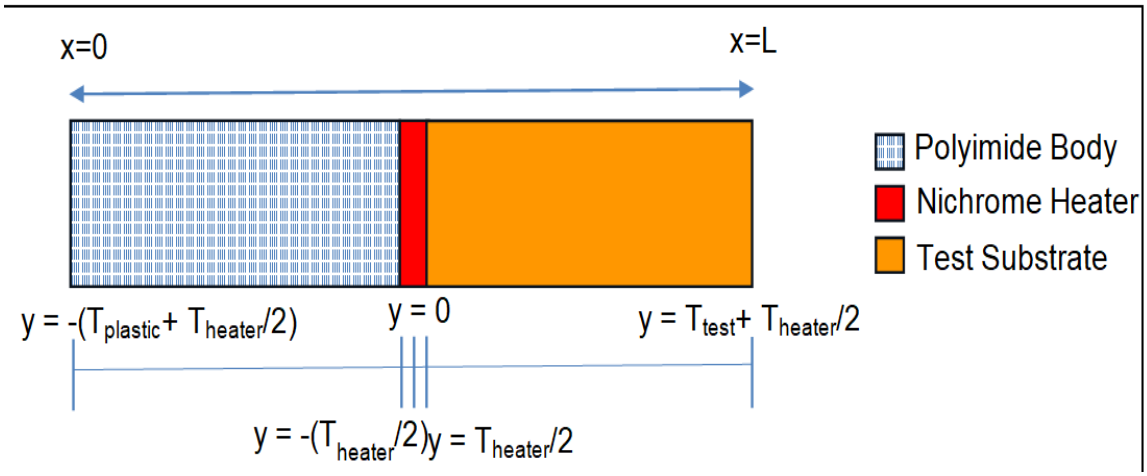

Figure 4: Abstracted representation of the multi-layered continuous 1D domain of the model (not to scale).

The spatiotemporal domains were discretised to enable numerical analysis in finite steps. The spatial domain is represented by $x \in [0, L]$ divided into N intervals, $x_i = i\Delta x$, where $i = 0,1,2 \ldots N$ and $\Delta x = \frac{L}{N}$. The quantity L is the total spatial domain length. A coordinate y was also defined, whose origin is located at the centre of the nichrome heating wire, with the negative direction extending into the polyimide body domain and the positive direction extending into the test substrate domain.

The temporal domain is represented by $t \in [0, t_{end}]$ divided into M intervals, $t_i = i\Delta t$, where $i = 0,1,2 \ldots M$ and $\Delta t = \frac{t_{end}}{M}$. The quantity t_{end} is the simulation end time.

Initial conditions of the system are required for the entire spatial domain. For this baseline comparison a uniform temperature of $T(0, t) = 25°C$ was considered sufficient.

Adiabatic boundary conditions are required at both the left and right boundary, expressed as Neumann type conditions:

$$-k_i \frac{\partial T(0,t)}{\partial x} = 0$$

$$-k_i \frac{\partial T(L,t)}{\partial x} = 0$$

Implicit assumptions made by the model include full thermal contact between substrate and material and isotropic thermal properties.

Figure 5 below shows the baseline surface plot for the case where the test substrate is polyimide; identical to the body material. This was chosen as the baseline because the analytical result is known and should be a 1:1 heat split ratio producing a quasi-Gaussian temperature profile around the centre of the heating wire domain.

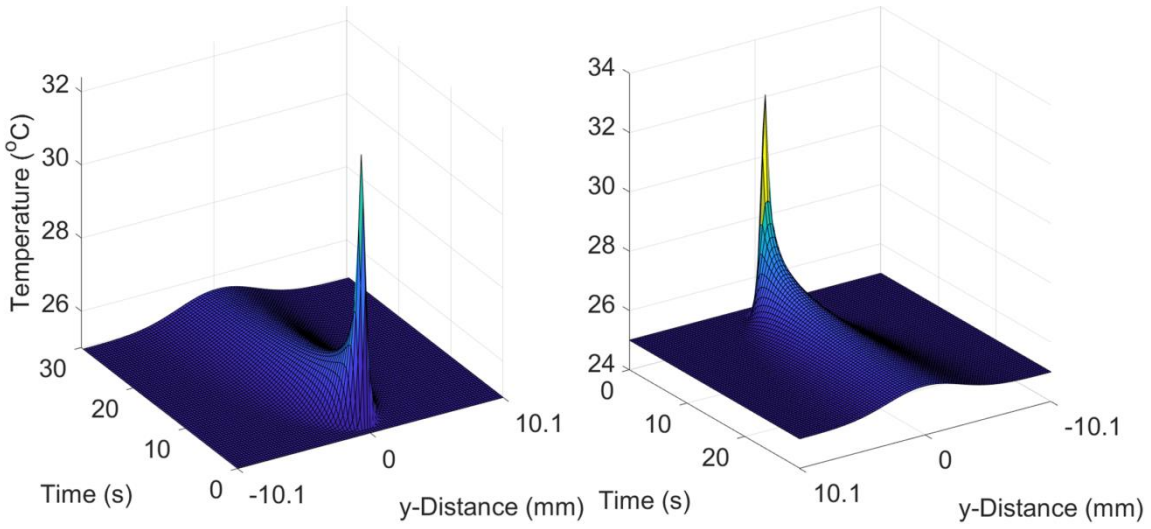

Figure 5: Surface plots of the polyimide test substrate baseline case detailing the temperature changes over time and space (y coordinate system).

As expected, the entire spatial domain begins at the initial temperature and after the delay period, sharply rises to a peak temperature of 32.4°C. This temperature was a result of later tuning of the input power to achieve the required 42°C surface temperature with a single crystal diamond substrate. On the ceasing of the pulse, the temperature around the heating wire falls sharply as the heat flux diffuses outward towards the polyimide body domain and test substrate domain. As both domains have identical material properties, the temperature distribution is symmetric around the heating wire location as expected, indicating a 1:1 heat split ratio. **Figure 6** highlights the symmetry of the baseline case for the material interfaces immediately after the elimination of the source term, and plots the same profiles for all other materials listed in **Table 1.**

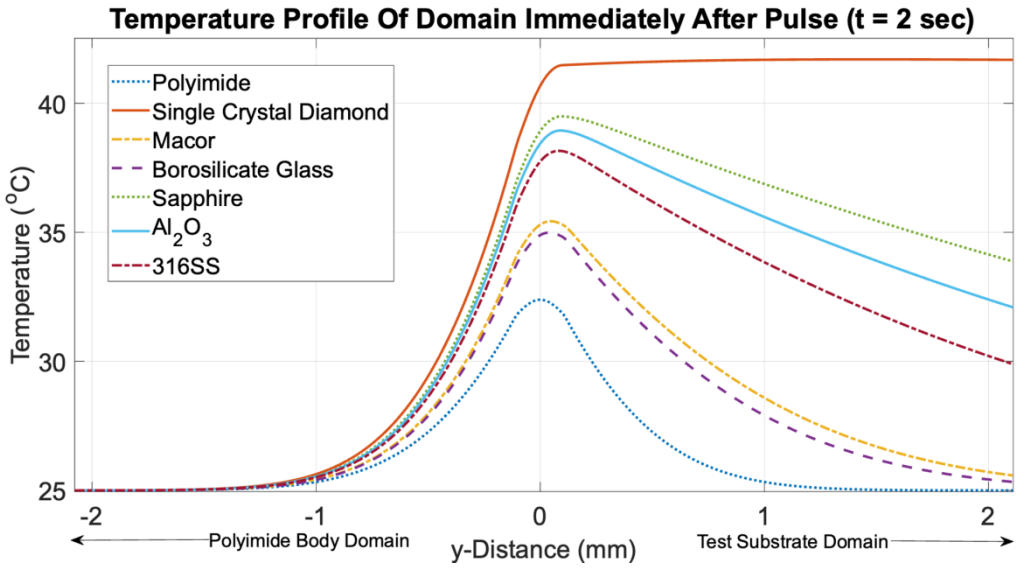

Figure 6: Temperature profile around the central nichrome heating wire (y = 0 mm) immediately following the thermal pulse. The y-coordinate system is used spatially, with the polyimide body domain and test substrate domain indicated by arrows below the plot.

The temperature ranking has polyimide last, followed by borosilicate glass, Macor, 316SS, Al_2O_3, sapphire, and finally single crystal diamond. As the volumetric power delivered to the heating wire is identical in all cases, we can conclude that less current (and therefore less power) is required to achieve the target temperature with single crystal diamond compared to all other candidate materials. Furthermore, the single crystal diamond temperature profile is more uniform than all others, indicating the potential for controlled heating across the sensor-skin interface, and the elimination of dangerous hotspots and consistent thermal contact.

Figure 7 converts the temperature profiles into heat split ratios by taking the spatial temperature derivative at the material interfaces, multiplying by the relevant material thermal conductivity, and calculating the ratio of the two values. Due to the inclusion of the thermal conductivity, this can significantly alter the ordering of the candidate materials, pushing those with greater thermal conductivity higher up the list.

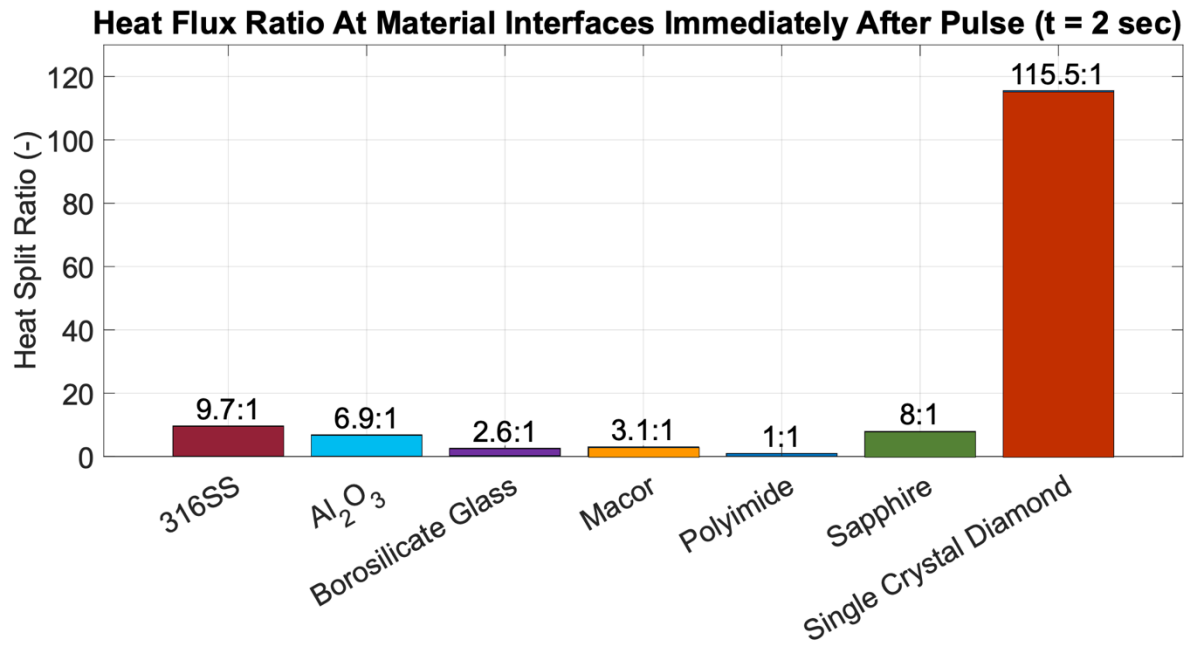

Figure 7: The heat split ratio for each test substrate around the material interfaces (y = -0.1 mm ; y = 0.1 mm) immediately following the thermal pulse.

As in **Figure 6**, single crystal diamond emerges as the preeminent material with a heat split ratio of 115.5:1, two orders of magnitude greater than 316 stainless steel (9.7:1) in second place. This highlights that greater heat split ratio does not necessarily translate to greater temperature due to the difference in the thermal capacity of the materials (density multiplied by specific heat capacity). Section 3.2 results demonstrate that single crystal diamond acts as a 'thermally transparent' substrate, with its exceptionally high thermal conductivity (1900 W/mK) rapidly distributing heat and preventing dangerous hotspots. This creates controlled, uniform heating at the skin interface - crucial for safe medical thermal sensing. In contrast, materials with lower thermal conductivity create localized heating that could damage tissue while providing unreliable readings. Diamond is thermally transparent which makes it optimal for skin cancer detection sensors where precise, safe thermal control is essential.

Temperature Safety Considerations

Temperature safety represents a critical design constraint for clinical sensors. The maximum allowable temperature at the surface of the skin is 42°C and therefore this has to be the upper limit [9]. For the thermal product sensor, the anticipation is that the surface temperature of a patient is approximately 20°C - 25°C and a step change to 42°C will be achieved at the sensor interface. This gives approximately 20°C temperature difference which is sufficient to evaluate the thermal product.

Sensor Conceptual Architecture

The probe specification is for a 2 mm diameter x1 mm thick single crystal diamond disc **(Figure 8).** These dimensions were chosen based on the thermal and mechanical interface with patient skin and the thermal response predicted using the 1D model **(Figure 6).** It is worth noting that preliminary sensors were manufactured with 1mm diameter diamond; however, these were found to be uncomfortable for the patient due to the greater contact pressure. The 2 mm diameter diamond was considered acceptable to achieve the target resolution for a typical mole size. However, if a 1mm sensor was required for a very small mole, this could be produced. An 80-micron K-type thermocouple for direct temperature measurement is brazed onto the rear of the diamond using a proprietary silver-based braze material. This is conducted at an approximate temperature of 750°C with the diamond in either vacuum or in the presence of an argon environment to ensure the diamond does not re-graphitise. To provide the heating pulse a fine wire heating element is manufactured and bonded to the rear of the diamond. The diamond is then placed on a polyimide pedestal for the construction of the probe body. This is engineered to be powered from a 5V capacitor for duration between 0.1 and 1 second time interval during which time the diamond reaches a temperature approaching 42°C when in contact with human skin.

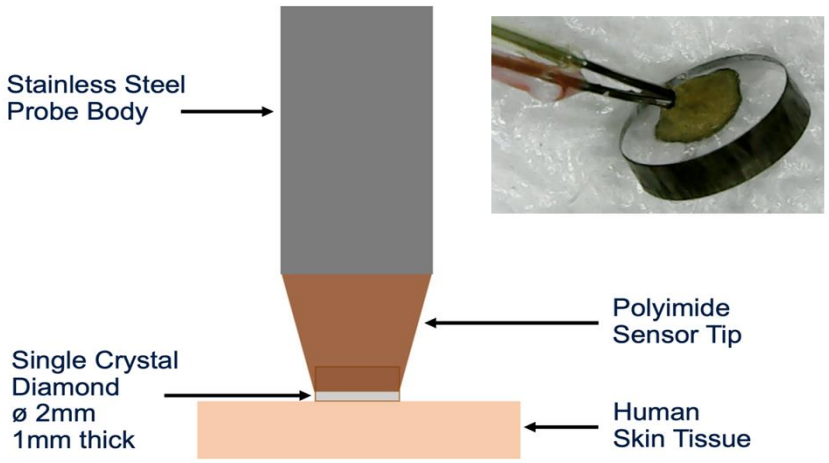

Figure 8: Latest single crystal diamond sensor schematic, including an inset photo of an actual thermocouple brazed to the diamond disc.

Temperature Measurement Method

Temperature measurement at the rear of the diamond requires a fast-response sensor to follow the thermal changes. Several sensor types could be considered, including platinum thin-film gauges, thermocouples, thermistors, or infrared devices. The disadvantage of thin-film gauges is that they do not measure temperature directly but instead rely on

resistance change under constant current, requiring calibration via the temperature coefficient of resistance. A standard K-type thermocouple with a bead size between 25-100 µm can alternatively be brazed to the rear of the diamond, offering direct temperature measurement when combined with a cold-junction chip and amplifier (e.g., AD-8497C) which has a high accuracy. The bead size should be kept small to preserve frequency response given the measurement time will be under a second.

Another option is medically approved micro-thermistors, such as the Semitec F-Micro or JT series, which offer very small sensing elements and hence a rapid thermal response. In this case, temperature is measured through resistance changes with temperature. A further possibility arises from the transparency of single-crystal diamond to infrared transmission. An IR camera focused on the rear surface could measure the skin–diamond interface temperature. However, given the diamond's limited thickness (0.5–1 mm), the advantage of IR versus a thermocouple or micro-thermistor at the rear surface is likely marginal. For further details of this measurement methods see patent (UK patent application number 2510155.1).

Signal Conditioning and Electronics

The sensor incorporates dedicated signal-conditioning electronics for both thermocouple measurement and heater control. Temperature is measured via the AD-8497C chip (Analog Devices), which provides cold-junction compensation and amplification. This chip offers high accuracy, with an uncertainty of:

- Absolute gain error: ±0.5% of reading (Δgain error ±0.05%)
- Absolute offset error: ±0.5°C (Δoffset error ±0.05°C).

Its transfer function is 5 mV/°C for a K-type thermocouple. The amplified signal is digitised using a 24-bit ADC (ADS131) with a 0–1 V input range, corresponding to a 200°C measurement span. While the ADC supports digital gain (×1, 2, 4, 8, 16) for narrower ranges, it is operated in ×1 mode to preserve the 200°C span for other applications. This provides an effective conversion uncertainty of ±0.012°C.

The heater element is powered via a 5F, 6V supercapacitor (PTV-6R0V505-R), which allows delivery of ~8–12W within a fraction of a second. This enables the probe to achieve a 20 °C temperature rise in ~0.25s.

Pulse timing is synchronised with the end-of-conversion pulse from the ADC, which is crystal clocked. This ensures highly accurate timing, limited only by clock jitter (sub-nanosecond).

The current prototype electronics are housed on a 50 mm × 25 mm PCB (1.6 mm thick) with components mounted on both sides. The largest component is the 11 mm thick supercapacitor, with connectors (~9.5 mm) and the power transistor (~6 mm) also contributing to height. The assembled thickness is ~22 mm, but could be reduced to ~18 mm with smaller components. In the next-generation design, the electronics will be further miniaturised and directly integrated into the probe body **(Figure 9),** reducing electrical interference by placing the electronics in closer proximity to the sensor tip.

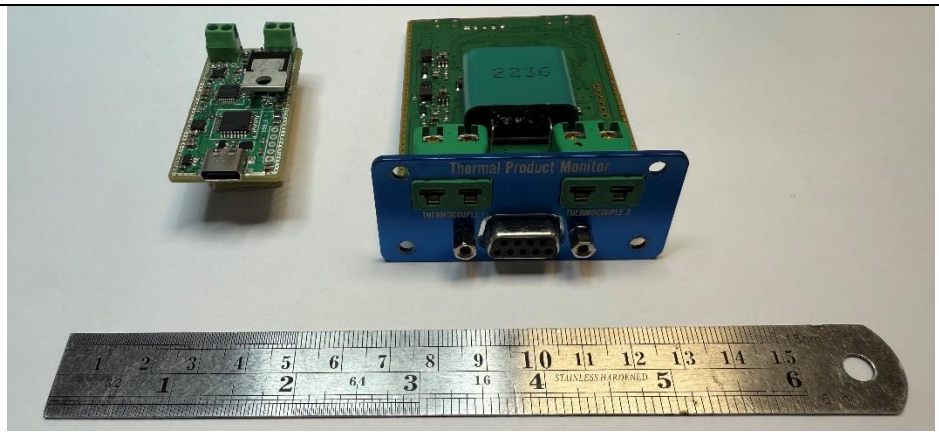

Figure 9: The latest miniaturised electronics (left) and the previous electronics (right).

Single Crystal Diamond – Response Time & Electrical Properties

The single crystal diamond is specifically engineered for this sensor by maximising the thermal properties and still providing a dielectric capability. The diamond is manufactured and shaped by Element Six (Oxfordshire, UK), using proprietary techniques for meeting the probe specifications. The diamond properties are approximately 55,954 J/(m^2 K $s^{0.5}$) thermal product, density of 3,515 kg/m^3, specific heat capacity of 510-540 J/kg-K, and thermal conductivity of 1,500-1,900 W/m-K. Information regarding the single crystal diamonds electrical properties– alongside other candidate materials for comparison – are detailed in **Table 2** below.

Table 2: Electrical properties of candidate materials selected for study.

Properties	Single Crystal Diamond	Al_2O_3 (99.5%)	HfO_2	Stainless Steel
Breakdown Voltage (MV/cm)	5	3.5	1	NA
Electrical Volume Resistivity (Ohm-cm)	10^{11}-10^{18}	10^{14}	10^{11}	$6.9x10^{-5}$

Figure 10 shows the predicted 80% rise time of the candidate materials listed in **Table 2.** A varied thermal pulse was applied to achieve an ~100°C step change in temperature for all materials.

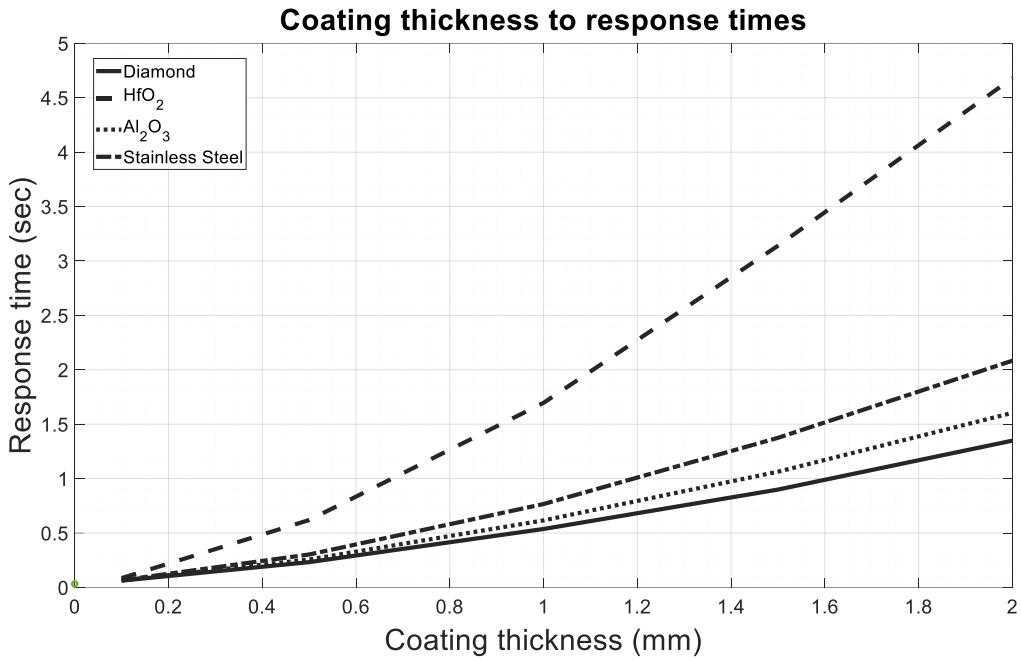

Figure 10: Thermal response time (80% rise time) of candidate probe materials vs. material thickness.

Modelling results demonstrate that Hafnium oxide exhibits the slowest response time (1 mm thickness; ~1.7 seconds), followed by stainless steel (1 mm thickness; ~0.75 seconds), Alumina (1 mm thickness; ~0.6 seconds), and single crystal diamond (1 mm thickness; ~0.55 seconds). Single crystal diamond therefore emerges as the leading choice from a thermal perspective. A fast response time indicates potential for excellent thermal coupling with the sample, which is critical for accurate determination of thermal properties.

In addition to the thermal properties, electrical properties were also examined, with breakdown voltage being treated as linear (a reasonable assumption over the thickness range studied). **Figure 11** details the breakdown voltage over a 'micron scale' range of substrate coating thicknesses for the candidate materials.

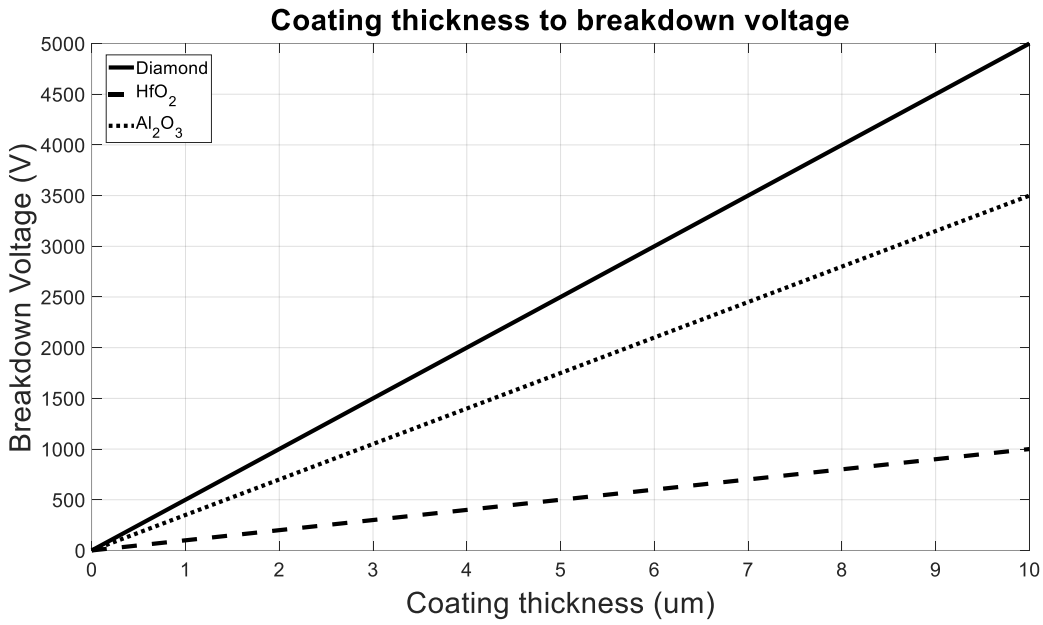

Figure 11: Breakdown voltage of candidate probe materials vs. material thickness.

It is clear from **Figure 11** that for all candidate materials any feasible thickness of substrate provides a large enough breakdown voltage to ensure safe operation, without the risk of sample (or patient) electrocution. Feasible thicknesses are within the 10^{-2}-10^{-1}mm range, providing a significant safety margin.

Sensor Operation Principle

The sensor fundamentally alters heat transfer pathways compared to previous designs. Heat applied at the back of the diamond substrate spreads immediately throughout the diamond due to its exceptionally high thermal product, then transfers into the skin tissue. This configuration eliminates sensor-patient contact whilst maintaining measurement sensitivity, allowing all major limitations to be addressed that were identified in thin film-based sensor studies, and operates very reliably through enhanced mechanical robustness and reduced contamination risks. Sensors designed and manufactured have undergone over 500 measurement points without deterioration with cleaning between measurements with isopropyl alcohol (IPA) wipes.

Three-Dimensional Thermal Analysis using ANSYS

Three-dimensional finite element analysis was conducted using ANSYS to model and understand the thermal gradients within the diamond sensor substrate and the interface between the biological tissues and diamond tip, as well as within the biological tissue. The computational model incorporated a multi-layer skin structure with cancerous lesions, realistic boundary conditions, temperature-dependent material properties, and transient thermal response analysis. The geometry can be seen in **Figure 12** below.

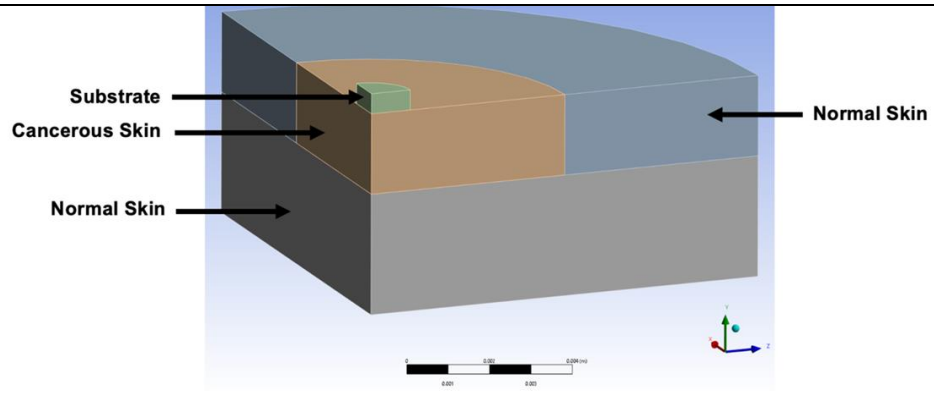

Figure 12: ANSYS setup showing substrate, cancerous skin layer surrounded by normal skin.

Mesh and Initial Conditions

The mesh element sizes were optimised for computational efficiency: substrate (0.1 mm), cancerous/tested skin (0.2 mm), normal skin around (0.3 mm), normal skin below (0.4 mm). Initial temperatures were set to physiological baseline levels: skin surface 34°C, cancerous-normal skin interface 36°C, normal skin bottom 37°C – values supported by literature indicating typical skin surface temperatures range around 32–35°C **[10].**

Temperature Distribution

An exponential decay of temperature with depth was applied, reflecting realistic heat dissipation in skin layers. Such behaviour aligns with bioheat modelling approaches, including variations on Pennes' equation and related analytical solutions, which demonstrate non-linear temperature gradients in layered biological tissue **[11].**

Parametric Study

A parametric analysis of diamond substrates of varying thicknesses – 1.0 mm, 0.5 mm, 0.2 mm, and 0.1 mm, with a constant diameter of 2 mm to examine the thermal response characteristics was performed. For experimental comparison purposes, water and air were also modelled. All simulations were performed with a constant heat input of 2×10^6 W/m². The heat input was evaluated to give a surface temperature of no more than 42°C. For all predictions the pulse heating was set for 5 milliseconds and thermal response was tracked over a 2-second simulation period.

Results

The thermal predictions for air show an increase in temperature during the pulse period from 22°C to approximately 36°C, whereas for water the equivalent temperature increase is 22°C to approximately 34°C, as shown in **Figure 13** for a substrate thickness of 0.5mm. Post pulse the thermal response for air can be approximated linearly and reduces by about 1°C over the 2 second cooling period. For the thermal response of water the response follows √t as anticipated from the 1D heat conduction equation, starting at approximately 34°C, rapidly falling in temperature for the first 0.5 seconds and then with a lower gradient over the remaining 1.5 seconds down to approximately 23°C. The √(ρck)of air is approximately 6 J/(m^2 K s$^{0.5}$), whereas for water (purified) is 1582 Ws$^{0.5}$/m^{2}K. The results show for a 0.1 mm thickness diamond a 60°C temperature difference resulting in a sensitivity [°C/TP] of 0.038°C/TP which is an order of magnitude better than any previous TP sensor results in the open literature.

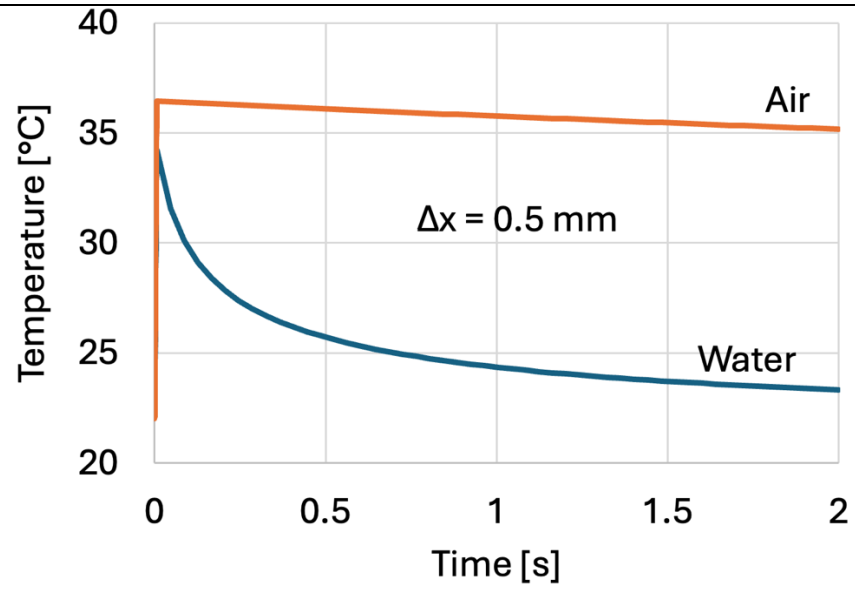

Figure 13: Results of thermal simulations using ANSYS for 0.5mm diamond thickness for air and water (thermal product difference ΔTP = 1576 J/(m^2 K s$^{0.5}$)).

These results show a significant improvement in the sensitivity as the diamond thickness was reduced from 0.5 mm to 0.1 mm. These values were chosen as lower than 0.1 mm is impractical for routine manufacturing. The thermal predictions indicate that a 5-times improvement can be achieved when reducing the diamond thickness from 0.5 mm to 0.1 mm. In terms of the skin cancer measurements this represents a step change performance in comparison to previous thin film-based sensors which had a 0.001037°C/TP sensitivity which was 10-times lower.

Table 3 gives a summary of the air and water predictions for all three diamond thicknesses and extends this further for cancerous and non-cancerous skin where a thermal product difference of approximately 380 J/(m^2 K s$^{0.5}$) was observed in the previous lesion study **[6].** The implications of this are that the detection of cancerous and non-cancerous tissue should be significantly easier with the new sensor concept if a sensor can be manufactured successfully with a 0.1 mm thickness. For a sensor of 0.5 mm thickness a temperature difference of 1.2°C would be observed which given the uncertainty in the temperature and logging system of approximately +/- 0.05°C would allow detection of cancerous tissue. This represents a significant improvement over the previous thin film-based sensor used in the study **[6],** where temperature differences of 0.05°C to 0.25°C were observed.

Table 3: Summary of air & water and normal & cancerous skin predictions for all three diamond thicknesses.

Diamond thickness	Temperature Difference Air and Water (ΔTP = 1576 J/(m^2 K s$^{0.5}$)) and Sensitivity	Temperature Difference Normal and Cancerous Skin (ΔTP = 380 J/(m^2 K s$^{0.5}$)) and Sensitivity
0.5 mm	12°C (0.008°C/TP)	1.2°C (0.00316°C/TP)
0.2 mm	30°C (0.019°C/TP)	2.6°C (0.00684°C/TP)
0.1 mm	60°C (0.038°C/TP)	4.4°C (0.0116°C/TP)

Discussion and Conclusions

The development of a diamond-tipped thermal sensor addresses the principal shortcomings of earlier thin-film sensor approaches. The modelling results demonstrate that the diamond's exceptionally high thermal product and conductivity create a near thermally transparent substrate, enabling controlled uniform heating at the skin interface. This overcomes the limitations of the Macor substrate-based sensors, where unfavourable energy split into the substrate led to significant heat losses. The distribution with diamond/polyimide is ~115.5:1 in favour of the heat flow into the diamond and hence the skin tissue.

The three-dimensional finite element modelling confirmed that diamond thickness strongly influences sensitivity, with thinner substrates (0.1–0.2 mm) producing an order-of-magnitude gain in °C/TP sensitivity compared with 0.5 mm substrates. These predicted sensitivities substantially exceed the 0.001037°C/TP achieved with thin-film sensors in previous clinical trials [DeGiovanni et al.], indicating that detection of small differences in thermal product between normal and cancerous skin ($\Delta TP \approx 380$ J/(m^2 K s$^{0.5}$)) should be significantly improved with a margin of safety over the system uncertainty.

Diamond also addresses several practical limitations of thin films. Its dielectric properties eliminate the need for external electrical isolation, while its hardness and chemical stability allow repeated cleaning and sterilisation without degradation. Furthermore, diamond's transparency opens the possibility for optical or IR-based temperature monitoring, although the advantage relative to thermocouples or micro-thermistors may be marginal given the substrate thicknesses used here.

Acknowledgements

The authors acknowledge Principal Technologies Inc. for funding the skin cancer research.

Dr Santonu Ghosh from Element Six UK Ltd. is acknowledged for the assistance provided for the diamond materials. Sunny Chana and Jamie Dean from Oxford University are acknowledged for their contributions for the manufacturing of the sensor parts.

References

1. Cancer Research UK. Melanoma skin cancer statistics. 2024.
2. Ethna McFerran et al. "Skin in the game: The cost consequences of skin cancer diagnosis, treatment and care in Northern Ireland". J Cancer Policy. 2024:39:100468.
3. NHS England. National Cost Collection for the NHS. Reference Costs. 2024.
4. Nick N, et al. "Thermal Product Sensing: Simulations and Experiments of a Novel Biosensor for Quantitative Thermal Property Measurement of Biological Tissues". Mega J Case Rep. 2025;8(6):2001-2019.
5. Nick N, et al. "Machine Learning Classification of Skin Lesions Using Thermal Product Biosensing: A Preliminary Diagnostic Approach". Mega J Case Rep. 2025;8(6):2001-2011.
6. DeGiovanni C, et al. "Thermal Product Sensor: A potentially new diagnostic tool in the detection of skin malignancy". Medical Research Archives. 2024.
7. P Sains, KS Chana, V Sridhar, MS. Sajid. Pilot study on an innovative biosensor with a range of medical and surgical applications. BMC Res Notes. 2018;11(1):81.
8. Sridhar, V, Chana, KS, & Singh, D. "Computational and Experimental Study

of a Platinum Thin-Film Based Oil Condition and Contamination Sensor." Proceedings of the ASME Turbo Expo 2017: Turbomachinery Technical Conference and Exposition. Volume 6: Ceramics; Controls, Diagnostics and Instrumentation; Education; Manufacturing Materials and Metallurgy. Charlotte, North Carolina, USA. June 26–30, 2017. V006T05A013. ASME.

9. Tiziana Mifsud et al. "The Effects of Skin Temperature Changes on the Integrity of Skin Tissue: A Systematic Review". Adv Skin Wound Care. 2022;35(10):555-565.
10. Chan Mi Lee, Seon-PilJin, EunJin Doh, Dong Hun Lee, Jin Ho Chung. Regional Variation of Human Skin Surface Temperature. Ann Dermatol. 2019;31(3):349-352.
11. Qian Zhang et al. "Characterization of Temperature Profiles in Skin and Transdermal Delivery System When Exposed to Temperature Gradients In vivo and In Vitro". Pharm Res. 2017;34(7):1491-1504.
12. TR Gowrishankar, Donald A Stewart, Gregory T Martin, James C Weaver. Transport lattice models of heat transport in skin with spatially heterogeneous, temperature-dependent perfusion. Biomed Eng Online. 2004;3(1):42.

Citation of this Article

Nick N, Kirkup J and Chana K. High-Sensitivity Diamond-tipped Thermal Sensor for Non-Invasive Skin Cancer Detection: Development and Validation – Part A. Mega J Case Rep. 2025;8(9):2001-2017.

Copyright